Pain Physician 2025; 28:E347-E357 • ISSN 2150-1149

Phantom Study

Applying a Preoperative Planning Method Based on 3D Artificial Intelligence-generated Lumbar Models in Transforaminal Puncture: A Phantoms Study

Zhihai Su, MD[1], Chengjie Huang, MD[1], Zhifei Cui, MD[1], Yunfei Wang, MD[1], Wencong Zhang, PhD[2], Lei Zhao, PhD[3], Shumao Pang, PhD[4], Naiwen Zhang, MD[5], Libin Liang, PhD[6], Zhen Yuan, PhD[7], Qianjin Feng, PhD[2], Xiang Liu, MD[1], Tao Chen, MD[1], and Hai Lu, PhD[1]

From: [1]Fifth Affiliated Hospital of Sun Yat-sen University, Department of Spinal surgery, Zhuhai, Guangdong, P.R. China; [2]School of Biomedical Engineering, Southern Medical University, Guangdong Provincial Key Laboratory of Medical Image Processing Guangzhou, Guangdong, P.R. China; [3]School of Biomedical Engineering, Guangdong Medical University, Dongguan, Key Laboratory of Medical Electronics and Medical Imaging Equipment, Dongguan, P.R. China; [4]School of Biomedical Engineering, Guangzhou Medical University, Guangzhou, Guangdong, P.R. China; [5]Institute of Medical Robotics, School of Biomedical Engineering, Shanghai Jiao Tong University, Shanghai, P.R. China; [6]Key Laboratory of Biomedical Information Engineering of Ministry of Education, Department of Biomedical Engineering, School of Life Science and Technology, Xi'an Jiaotong University, Xi'an, Shanxi, P.R. China; [7]Faculty of Health Sciences, University of Macau, Taipa, Macau SAR, P.R. China

Address Correspondence:
Hai Lu, PhD
Fifth Affiliated Hospital of Sun Yat-sen University, Department of Spinal surgery, Zhuhai, Guangdong, P.R. China
E-mail: lvhai@mail.sysu.edu.cn

Disclaimer: Z. Su, C. Huang, and Z. Cui contributed equally to this work and should be considered as co-first authors. X. Liu, T. Chen, and H. Lu contributed equally to this work. This study received funding by the R&D project of Pazhou Lab (Huangpu) under Grant 2023K0604; the Joint Funding Scheme 2022 for Scientific Research Projects (FDCT-GDST Projects) by the Science and Technology Development Fund of Macau and the Department of Science and Technology of Guangdong Province (2022A0505020019 and 0056/2021/AGJ); the Macau Young Scholars Programme (AM2023022); the Guangdong Climbing Plan (pdjh2023b0011); National Natural Scienecs Foundation of China (62371146); and the Fundamental Research Funds for the Central Universities (xzy012022036).

Background: Transforaminal puncture is a critical element of lumbar transforaminal epidural steroid injections used to manage lumbar radicular pain. Numerous challenges persist, owing to the intricate 3-dimensional (3D) anatomy of the spine and the delicate nature of the neurovascular structures involved. Consequently, performing the puncture expeditiously, precisely, and safely is imperative. Although numerous scholars have explored methods for reconstructing 3D lumbar models from patient data, the practical application of these models in puncture path planning for transpedicular procedures remains limited. Approaches based on artificial intelligence offer promising advantages for constructing patient-specific 3D models to facilitate puncture pathways planning.

Objective: In this experimental study, we proposed a preoperative planning method utilizing 3D artificial intelligence-generated lumbar models to improve the accuracy and efficiency of the transforaminal puncture process.

Study Design: A phantoms study.

Setting: The Fifth Affiliated Hospital of Sun Yat-sen University, Zhuhai, P.R. China.

Methods: A total of 24 puncture trials utilizing 12 phantom models were independently conducted by 2 surgeons, employing our developed preoperative planning method and conventional fluoroscopy. After one month, one of the surgeons repeated the procedure. Puncture error, characterized by the discrepancy between the preoperative planning puncture target and the actual postoperative needle puncture point (measured in millimeters), as well as puncture procedure duration (measured in minutes), were evaluated by comparing the newly developed preoperative planning method with the traditional fluoroscopy method employed in the transforaminal puncture process.

Results: The average puncture error associated with the preoperative planning method was significantly lower than the conventional fluoroscopy method (3.33 ± 0.73 mm vs 5.25 ± 0.92 mm, $P < 0.001$). Additionally, the average puncture time of the preoperative planning method was significantly shorter than the conventional fluoroscopy method (7.29 ± 0.95 minutes vs 11.48 ± 1.27 minutes, $P < 0.001$).

Limitations: Our study used a small number of models; additional clinical trials are required to validate our preoperative planning methods.

Conclusion: The preoperative planning method utilizing 3D artificial intelligence-generated lumbar models for transforaminal puncture demonstrated superior accuracy and efficiency in phantom trials over the traditional fluoroscopic method. This newly developed preoperative planning technique has the potential to significantly improve the accuracy and efficiency of the transforaminal puncture process.

Conflict of interest: The manuscript submitted does not contain information about medical device(s)/drug(s). Each author certifies that he or she, or a member of his or her immediate family, has no commercial association (i.e., consultancies, stock ownership, equity interest, patent/licensing arrangements, etc.) that might pose a conflict of interest in connection with the submitted article.

Article received: 01-02-2025
Revised article received: 01-03-2025
Accepted for publication: 03-05-2025

Free full article: www.painphysicianjournal.com

Key words: Lumbar radicular pain, transforaminal epidural steroid injections, puncture, 3D model, artificial intelligence, AI, preoperative planning

Pain Physician 2025: 28:E347-E357

Transforaminal puncture (TP) is a key component of lumbar transforaminal epidural steroid injections for lumbar radicular pain (1,2). Mobile fluoroscopy (C-arm) units are commonly used in TP (3). Numerous challenges remain, owing to the complexity of the 3-dimensional (3D) spinal anatomy and the sensitive nature of neurovascular structures (4,5). A surgeon must understand the 3D anatomy of the lumbar spine and have experience with open surgery; otherwise, both the patient and surgeon will be exposed to excessive radiation during the puncture (6). Moreover, an inaccurate puncture can injure vessels, nerves, dura, and abdominal organs (7). Therefore, finding and puncturing quickly, accurately, and safely is essential.

The improvement in TP comes from the knowledge of 3D lumbar anatomy, especially Kambin's triangle (8). The Kambin triangle, which is an anatomical corridor made by the exiting nerve root, dural canal, superior endplate of the lower lumbar vertebra, and superior articular processes, is an essential pathway for TP (9). However, these anatomic structures may be different and are influenced by gender, increasing age, and pathological factors (10). In addition, the ability of surgeons to think spatially is closely linked to TP success and lumbar radicular pain treatment. Surgeons always require high spatial thinking in the TP process to convert 3D images or models from intraoperative 2D images combined with preoperative computed tomography (CT) or magnetic resonance (MR) images. Therefore, one of the significant challenges in TP is constructing a 3D lumbar model of real structures, including the Kambin triangle, in patients.

Artificial intelligence (AI)-based approaches have potential advantages in building 3D models of patients (11,12). Although many scholars have investigated how 3D lumbar models are reconstructed from patient data, such as x-rays(13), CT (14), and MR images (15), few surgeons apply 3D model reality to puncture path planning in TP. Previous studies on 3D lumbar models based on deep learning have only assessed TP ideal angulation range (14) and the difficulty of percutaneous endoscopic lumbar discectomy (16,17). Unfortunately, these methods cannot be utilized directly to plan and implement a puncture path in a TP. A preoperative planning method is currently lacking to fully utilize 3D lumbar models based on deep learning to prepare a puncture path in transforaminal epidural steroid injections.

In our experimental study, we proposed a preoperative planning method based on 3D AI-generated lumbar models to improve the accuracy and efficiency of the TP process. Compared with the conventional fluoroscopy method of TP usually used in clinics, the discrepancy between the preoperative planning puncture target (Pt) and actual needle puncture point (Pa) and the puncture time was used to assess and establish the validity of this new method.

Methods

Twelve phantom models created using 3D lumbar models, which were generated using AI from the MR images of patients, were used in our study (15). Approval for this study was obtained from the Medical Ethics Committee of the Fifth Affiliated Hospital of Sun Yat-sen University. Due to the secondary data analysis of the MR images, additional informed consent was not required.

Creating Phantom-Based 3D Lumbar AI-Generated Models

The following procedures were used to create the phantom models.

1) We inputted the lumbar MR images of patients (DICOM format) into our previously developed automated MR image segmentation network (15), aiming to output lumbar spine masks (including bones, skin, dura mater, discs, and nerve roots). The detailed automatic segmentation Dice Coefficient scores of the masks are listed in Table 1.
2) The lumbar spine masks were imported into Mimics Innovation Suite software (NIHA Solutions) to create a 3D model (Fig. 1A), which was then modified based on MR images and printed by Zhuhai Seine Technology Co., Ltd.
3) Two relevant parameters were measured using Mimics software to determine the specific location of each 3D lumbar model within the foaming mold. Based on these parameters, the 3D lumbar models were independently positioned into the foaming mold to create a phantom model (Fig. 1B).

A New Planning Plugin

A new planning plugin developed and integrated into 3D Slicer software (www.slicer.org) was used to plan the puncture path and calculate its key parameters to assist surgeons in improving the transforaminal epidural steroid injection's accuracy and efficiency. The specific operational process of the planning plugin was as follows (Fig. 2):

1) The 3D lumbar model was initially visualized using 3D Slicer software. Subsequently, the Pt and projection points of the spinous process of the inferior vertebra (Ps) were marked on the 3D lumbar model. The transverse, coronal, and sagittal planes of the 3D lumbar model were determined using Ps as a reference point.

2) The 3D lumbar model was rotated to determine the appropriate TP angle. Subsequently, a pathway 3 mm in diameter was generated to reach Pt and avoid any obstacles to the 3D lumbar model using our developed planning plugin. The planning plugin was applied in order to automatically calculate these puncture parameters, including the transverse plane angulation α, coronal plane angulation β, sagittal plane angulation θ, the distance between the skin entry point and midline (Dp), and height between the skin entry points (Pe) and Ps (Hp) of the pathway.

For all phantom models, the intersection between the medial margin of the pedicle and the superior posterior endplate of the inferior vertebra was considered Pt for transforaminal epidural steroid injections.

A Preoperative Planning Method Based on 3D AI-generated Lumbar Models for Transforaminal Puncture

Before TP, every surgeon was required to plan an appropriate puncture pathway on both sides of the intervertebral foramen in order to determine the relevant parameters (including α, β, θ, Dp, and Hp) using our developed planning plugin (Fig. 2). Based on these parameters, the skin puncture point and angle were marked on the corresponding phantom model which was secured prone to a radiolucent table. Subsequently, the puncture angle during the TP process was adjusted under anteroposterior and lateral C-arm fluoroscopy in order to ensure that the needle tip reached the closest area of the Pt, as Pa. The puncture time was recorded at TP completion, and a 3D

Table 1. *Dice Coefficient score of automated lumbosacral magnetic resonance image segmentation.*

Dice score and cases		Lumbosacral structures							
		L4	L5	S1	Disc	Nerves	Iliac Bone	Skin	Mean
L4/L5	Case 1	0.888	0.897	N/A	0.896	0.747	N/A	0.893	0.864
	Case 2	0.928	0.921	N/A	0.905	0.805	N/A	0.915	0.895
	Case 3	0.927	0.924	N/A	0.918	0.868	N/A	0.909	0.909
	Case 4	0.935	0.935	N/A	0.910	0.856	N/A	0.881	0.904
	Case 5	0.951	0.940	N/A	0.935	0.876	N/A	0.915	0.923
	Case 6	0.930	0.919	N/A	0.934	0.871	N/A	0.918	0.914
L5/S1	Case 7	N/A	0.934	0.949	0.907	0.821	0.908	0.869	0.887
	Case 8	N/A	0.947	0.944	0.924	0.848	0.858	0.909	0.897
	Case 9	N/A	0.944	0.946	0.916	0.806	0.909	0.855	0.883
	Case 10	N/A	0.933	0.948	0.902	0.873	0.940	0.884	0.908
	Case 11	N/A	0.942	0.922	0.919	0.853	0.919	0.908	0.902
	Case 12	N/A	0.947	0.950	0.947	0.828	0.892	0.906	0.900

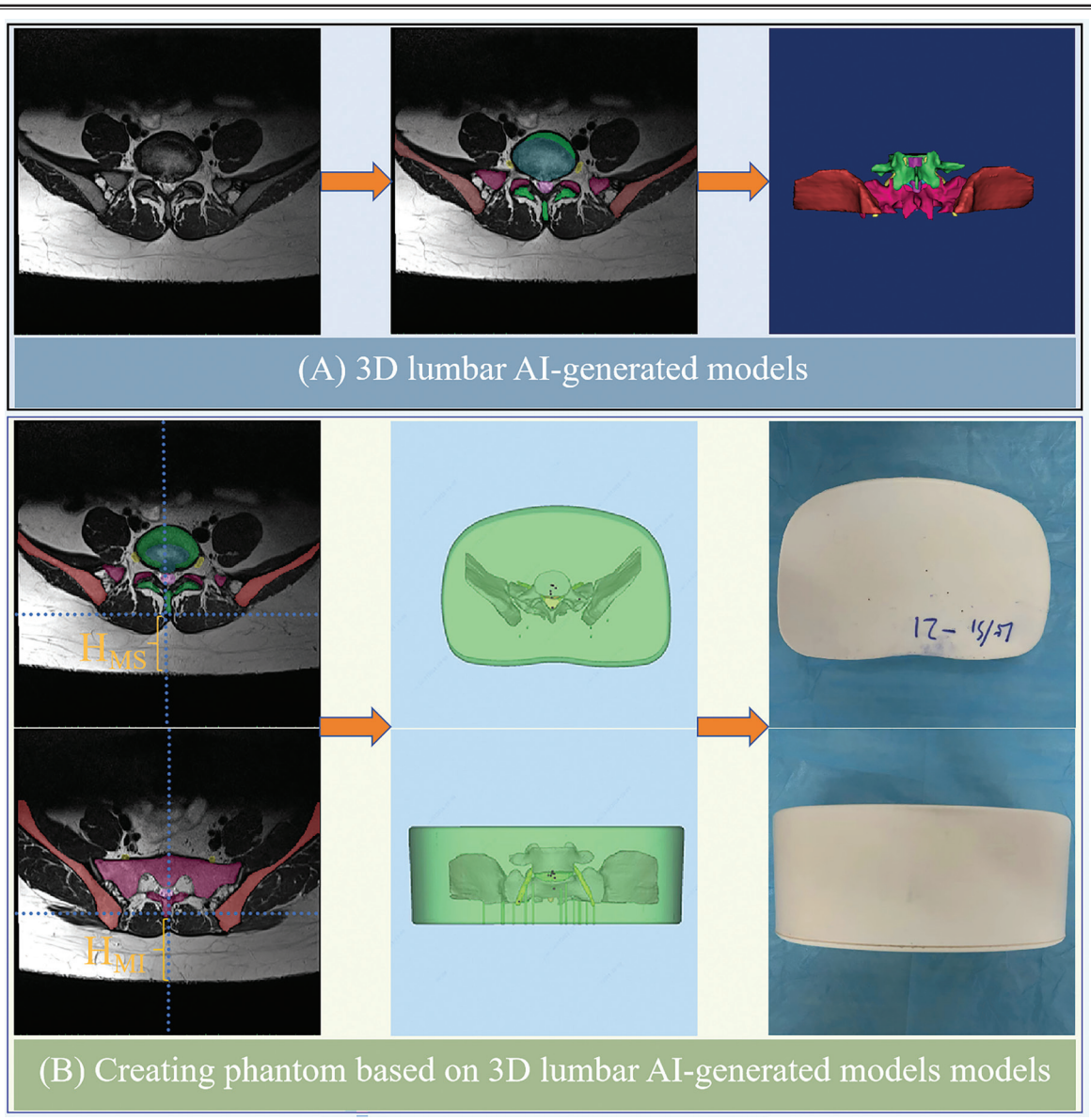

Fig. 1. *Schematic of the workflow adopted for creating phantom based on 3D lumbar AI-generated models. A: 3D lumbar AI-generated models from patients' MR images. B: phantom models created by 3D lumbar AI-generated models. HMS = the shortest distance from the superior spinous process to the skin. HMI = the shortest distance from the inferior spinous process to the skin.*

C-arm scan was performed on the phantom model to calculate the Euclidean distance between Pt and Pa, which served as a puncture error (Fig. 3).

A total of 24 puncture trials were conducted on 12 phantom models by 2 surgeons (surgeons A1 and B); all trials were performed independently. One of the surgeons repeated the procedure after one month (surgeon A2).

The Conventional Fluoroscopy Method for Transforaminal

All phantom models were secured prone to a radiolucent table. A 23 cm, 17G spinal needle was advanced into the closest area of the Pt (Pa) around the intervertebral foramen, based on the surgeon's experience. The needle tip position was checked and adjusted repeatedly using anteroposterior and lateral C-arm fluoroscopy. At

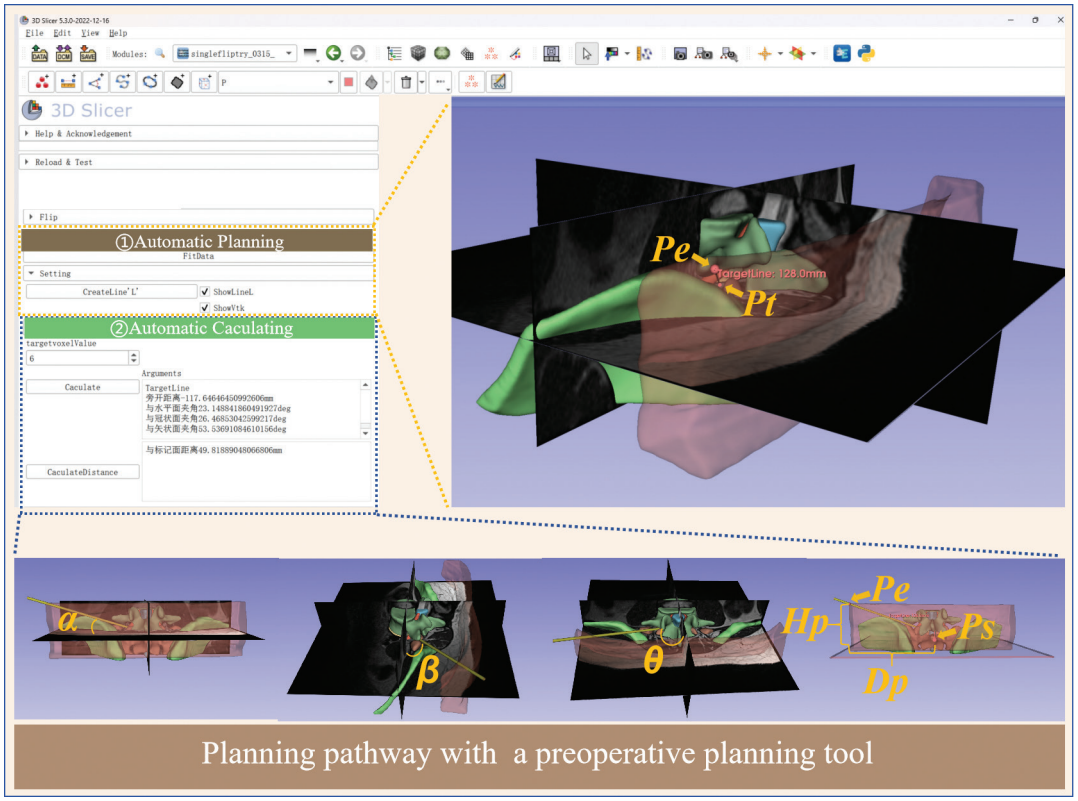

Fig. 2. *The developed planning tool for planning an appropriate puncture pathway and calculating puncture parameters on a 3D AI-generated lumbar model.* ①*Automatic planning module for puncture pathway,* ②*Automatic caculating module for puncture pathway. Pe = skin entry point, Pt = puncture target, Ps = the projection point of the spinous process of the inferior vertebra, Dp = the distance between the skin entry point and the midline, Hp = the height between skin entry point and the projection point of the spinous process of the inferior vertebra,* α *= transverse plane angulation,* β *= coronal plane angulation,* θ *= sagittal plane angulation.*

TP completion, the puncture time was recorded, and 3D C-arm fluoroscopy scanning was performed on the phantom model in order to calculate the Euclidean distance between Pt and Pa, which served as a puncture error.

A total of 24 puncture trials were conducted on 12 phantom models by 2 surgeons (A and B); all trials were performed independently. One of the surgeons repeated the procedure after one month.

Statistical Analysis

All data were analyzed using IBM SPSS Statistics 26.0 (IBM Corporation). Experimental measurements were reported as mean (SD). Statistical analysis of the measurement data was conducted using a t test. Pearson correlation analysis was used to evaluate the potential correlation between puncture time and puncture error for the 2 methods. A $P < 0.05$ was considered statistically significant.

Results

A total of 24 transforaminal punctures were conducted on 12 phantom models for each of the 2 methods, with 12 punctures performed at the L4/5 intervertebral foramen and 12 at the L5/S1 intervertebral foramen. The results of the relevant parameters (including α, β, θ, Dp, and Hp) for the 2 methods are presented in Tables 2–4.

In our study, the average puncture time and error for the 2 surgeons employing the preoperative planning method were lower than those associated with the conventional fluoroscopy method. Average puncture time using the preoperative planning method and the conventional fluoroscopy method were 7.29 (0.95) minutes and 11.48 (1.27) minutes, respectively ($P < 0.001$). The average puncture errors were 3.33 (0.73) mm in the preoperative planning method and 5.25

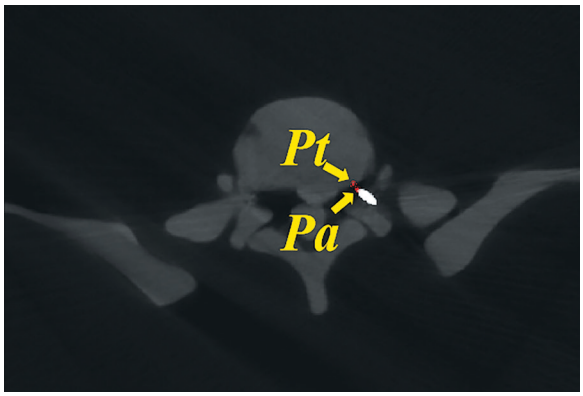

Fig. 3. *Schematic diagram of measuring the actual needle puncture point (Pa) and the puncture target (Pt).*

(0.92) mm in the conventional fluoroscopy method ($P < 0.001$). Both puncture time and puncture errors for each surgeon (surgeon A1, surgeon A2, and surgeon B) using the preoperative planning method were lower than those using the conventional fluoroscopy method, as illustrated in Table 5.

The correlation analysis between puncture time and puncture error showed that there were significant correlations for surgeon A1 (r = 0.704, $P < 0.001$), surgeon A2 (r = 0.703, $P < 0.001$), surgeon B (r = 0.553, $P < 0.001$), and the 2 surgeons (r = 0.825, $P < 0.001$), as shown in Fig. 4.

Discussion

The 3D models derived from patient imaging data

Table 2. *The results of the pertinent parameters for the 2 transforaminal puncture methods employed by surgeon A1.*

Cases and methods		The transforaminal puncture' parameters (Left)					The transforaminal puncture' parameters (Right)				
		α(°)	β(°)	θ(°)	Dp (mm)	Hp (mm)	α(°)	β(°)	θ(°)	Dp (mm)	Hp (mm)
Case 1	CF	87.09	54.59	32.69	149.49	30.06	73.07	62.35	35.65	98.63	19.66
	PP	80.19	59.12	34.95	131.73	29.31	75.87	53.92	37.46	108.52	16.20
Case 2	CF	75.90	63.51	30.55	154.44	56.47	82.83	49.91	41.00	116.08	32.21
	PP	76.91	59.12	30.87	144.14	54.57	82.59	52.94	41.53	111.45	35.06
Case 3	CF	88.65	58.36	29.23	139.59	20.21	89.50	50.41	42.09	104.60	10.93
	PP	85.20	57.25	29.85	132.35	4.32	84.95	52.05	41.76	106.90	28.45
Case 4	CF	76.26	63.19	28.63	158.59	57.67	77.22	51.05	43.79	105.75	48.40
	PP	77.72	64.40	30.43	156.74	61.75	77.57	49.20	42.50	108.39	43.72
Case 5	CF	79.52	64.95	25.29	183.69	31.52	77.74	52.35	42.66	108.77	50.64
	PP	82.85	56.26	31.45	154.79	33.41	77.65	57.15	39.81	120.94	49.34
Case 6	CF	79.62	57.23	33.93	127.40	48.59	75.46	55.10	39.40	125.12	57.85
	PP	77.66	52.70	37.60	120.63	52.17	75.21	57.42	38.87	125.54	58.69
Case 7	CF	76.77	50.73	41.43	126.79	47.32	75.24	53.37	41.72	126.79	47.32
	PP	75.55	47.27	47.46	114.08	44.92	77.61	54.73	37.53	116.76	49.18
Case 8	CF	78.05	53.60	37.34	125.20	52.67	75.53	63.81	31.86	135.15	56.80
	PP	76.57	57.71	34.01	135.10	61.47	72.31	60.42	36.99	124.01	61.57
Case 9	CF	80.03	56.58	33.55	134.71	45.09	79.03	56.50	37.49	116.02	48.82
	PP	78.03	58.42	33.15	135.17	52.78	77.67	55.18	38.79	124.56	47.98
Case 10	CF	78.64	52.33	37.75	143.76	39.63	78.71	52.00	42.62	124.50	49.50
	PP	78.21	49.10	42.01	138.00	50.74	78.78	55.28	39.25	134.84	41.37
Case 11	CF	75.57	57.60	33.89	136.05	51.45	70.14	51.76	47.31	104.45	58.09
	PP	75.97	55.40	29.16	131.96	36.94	70.87	57.93	48.62	100.30	69.68
Case 12	CF	71.77	47.47	45.56	109.19	55.21	73.13	58.02	39.86	116.84	48.45
	PP	75.03	54.34	36.49	140.35	52.20	70.45	54.34	36.49	140.35	52.20

L4/L5: Case 1 to Case 6, L5/S1: Case 7 to Case 12, CF = The conventional fluoroscopy method, PP = The preoperative planning method, α = transverse plane angulation, β = coronal plane angulation, θ = sagittal plane angulation, Dp = the distance between the skin entry point and the midline, Hp = the height between skin entry point and the projection point of the spinous process of the inferior vertebra.

Table 3. *The results of the pertinent parameters for the 2 transforaminal puncture methods employed by surgeon A2.*

Cases and methods		The transforaminal puncture' parameters (Left)					The transforaminal puncture' parameters (Right)				
		α(°)	β(°)	θ(°)	Dp (mm)	Hp (mm)	α(°)	β(°)	θ(°)	Dp (mm)	Hp (mm)
Case 1	CF	81.24	53.70	37.36	130.47	30.92	77.56	50.15	42.89	112.11	40.04
	PP	81.66	53.61	37.48	126.75	26.53	80.92	48.82	42.96	111.86	42.63
Case 2	CF	80.13	68.77	20.54	182.49	44.60	80.94	67.98	27.16	164.81	66.01
	PP	77.14	56.71	33.03	134.97	50.13	76.97	57.12	40.21	115.02	52.65
Case 3	CF	77.85	61.20	31.82	157.85	49.74	80.93	54.13	37.82	128.03	38.18
	PP	81.00	58.58	30.36	142.65	39.72	77.27	53.97	41.68	109.78	42.16
Case 4	CF	72.83	64.19	33.89	145.81	61.90	79.47	49.77	42.39	108.57	54.40
	PP	73.35	63.55	32.13	144.13	52.94	73.35	63.55	32.13	144.13	52.94
Case 5	CF	81.15	57.65	33.53	131.42	25.44	49.46	77.78	43.54	108.28	52.63
	PP	49.46	77.78	43.54	108.28	52.63	49.46	77.78	43.54	108.28	52.63
Case 6	CF	81.46	53.78	32.96	129.89	34.74	79.15	58.93	38.03	131.22	59.19
	PP	79.57	55.66	35.32	126.83	42.52	76.99	55.03	39.16	123.84	63.30
Case 7	CF	74.70	49.86	40.95	119.22	43.92	79.41	42.89	52.98	85.77	38.53
	PP	79.03	50.01	40.14	117.80	27.42	85.08	42.45	50.56	85.24	40.69
Case 8	CF	81.56	51.92	34.82	120.07	48.89	73.30	61.64	37.53	127.48	48.82
	PP	78.07	50.25	38.69	113.35	51.74	75.16	55.94	41.54	114.32	58.93
Case 9	CF	73.18	53.97	39.21	132.53	60.63	78.43	57.22	37.23	128.9	45.15
	PP	72.08	51.97	42.38	116.08	54.35	82.00	56.19	37.15	131.57	42.08
Case 10	CF	75.32	48.72	44.09	121.33	53.29	72.49	50.75	45.37	127.94	61.21
	PP	75.00	47.54	44.83	114.60	54.47	76.50	53.16	41.55	130.48	48.58
Case 11	CF	76.69	60.50	31.84	140.58	50.31	70.01	51.37	46.41	104.90	60.69
	PP	74.14	61.27	33.91	138.04	54.32	72.59	46.31	48.73	92.83	54.32
Case 12	CF	77.05	55.46	33.57	135.10	51.03	76.46	38.98	58.45	71.87	41.53
	PP	77.80	57.51	31.99	138.32	50.56	69.67	48.79	51.31	93.54	55.39

L4/L5: Case 1 to Case 6, L5/S1: Case 7 to Case 12, CF = The conventional fluoroscopy method, PP = The preoperative planning method, α = transverse plane angulation, β = coronal plane angulation, θ = sagittal plane angulation, Dp = the distance between the skin entry point and the midline, Hp = the height between skin entry point and the projection point of the spinous process of the inferior vertebra.

are instrumental in devising an appropriate surgical strategy, traditionally employed to enhance needle puncture precision, particularly TP. Our study explored the accuracy and efficacy of a preoperative planning approach using 3D AI-generated lumbar models for TP. The findings indicate the potential of this preoperative planning method to decrease puncture time and increase TP efficiency.

The conventional fluoroscopy method for TP predominantly relies on technical proficiency, clinical experience, comprehensive knowledge of lumbar anatomy, tactile feedback from surface anatomical landmarks, and the spatial awareness of the surgeon (18). Junior surgeons often require multiple punctures and fluoroscopy to position the needle accurately because of limited spatial imagination and clinical experience. This process can prolong their learning curve and risk injuring vessels, nerves, dura, and abdominal organs (7,18).

Over the past 10 years, new methods have been proposed to improve puncture accuracy and efficiency. Medical imaging system-assisted puncture techniques, such as the O-arm method (19), ultrasound method (20), CT-guided puncture method (21), and magnetic resonance imaging (MRI)-guided method (22), have been developed to accurately position the puncture needle at the optimal target site for TP. Nevertheless, MRI, CT, and O-arm machines are expensive and not routinely accessible in orthopedic operating rooms. Furthermore, ultrasound-guided needle puncturing requires an extended scanning duration and is constrained by limited reconstruction accuracy.

Owing to the widespread use of C-arm fluoroscopy machines in orthopedic operating rooms, fluoroscopy-

Table 4. *The results of the pertinent parameters for the 2 transforaminal puncture methods employed by surgeon B.*

Cases and methods		The transforaminal puncture' parameters (Left)					The transforaminal puncture' parameters (Right)				
		α(°)	β(°)	θ(°)	Dp (mm)	Hp (mm)	α(°)	β(°)	θ(°)	Dp (mm)	Hp (mm)
Case 1	CF	87.09	54.59	32.69	161.76	27.30	73.97	62.35	35.65	136.54	59.33
	PP	73.97	62.35	35.65	136.54	59.33	75.87	53.92	37.46	128.11	46.26
Case 2	CF	86.37	51.63	39.04	115.32	28.86	86.37	51.63	39.04	115.32	28.86
	PP	79.09	59.32	32.67	151.89	46.94	79.09	59.32	32.67	151.89	46.94
Case 3	CF	86.37	65.61	24.43	169.34	25.15	78.86	53.12	39.20	114.37	39.71
	PP	77.90	63.47	30.88	154.43	48.84	81.71	52.42	37.73	121.21	31.31
Case 4	CF	77.72	60.25	35.94	126.82	39.38	77.72	60.25	35.94	126.82	39.38
	PP	75.83	63.98	31.50	148.95	53.76	72.14	54.27	40.03	123.24	70.62
Case 5	CF	89.89	66.44	23.52	138.66	17.80	84.17	69.81	20.67	121.25	33.56
	PP	88.39	56.62	35.09	138.75	21.75	76.04	55.03	36.60	129.53	46.00
Case 6	CF	88.34	53.99	35.35	122.06	26.62	79.73	54.82	37.67	117.11	55.08
	PP	77.71	58.24	34.88	135.95	50.33	83.64	58.32	32.00	139.90	45.70
Case 7	CF	84.82	45.78	46.02	101.77	25.63	80.87	49.83	40.32	108.10	35.34
	PP	75.61	47.47	46.31	107.43	45.60	80.50	51.89	39.43	114.27	41.34
Case 8	CF	77.18	51.74	38.44	115.58	49.98	75.74	55.66	40.66	118.13	55.62
	PP	80.09	55.19	34.18	119.62	47.97	76.16	56.37	39.51	113.96	52.71
Case 9	CF	75.90	54.10	38.85	115.25	46.73	82.29	41.19	50.49	91.24	33.37
	PP	74.76	54.91	40.51	120.15	52.85	79.27	47.13	43.97	102.46	41.28
Case 10	CF	78.79	51.30	38.18	128.12	48.41	81.65	47.52	46.54	117.82	32.78
	PP	78.01	48.18	44.28	118.44	37.53	84.79	42.38	47.83	106.63	34.89
Case 11	CF	80.20	57.81	34.69	121.84	43.65	80.14	43.20	48.07	89.26	37.87
	PP	76.35	58.99	33.57	134.21	45.73	70.87	50.46	46.80	95.78	57.40
Case 12	CF	75.42	56.19	38.76	121.91	49.26	72.19	55.07	39.31	115.49	44.25
	PP	72.91	58.37	35.85	131.75	55.31	70.67	55.11	42.45	113.41	51.72

L4/L5: Case 1 to Case 6, L5/S1: Case 7 to Case 12, CF = The conventional fluoroscopy method, PP = The preoperative planning method, α = transverse plane angulation, β = coronal plane angulation, θ = sagittal plane angulation, Dp = the distance between the skin entry point and the midline, Hp = the height between skin entry point and the projection point of the spinous process of the inferior vertebra.

guided robotic systems for TP have garnered significant attention. However, these systems have some drawbacks, such as high cost and poor-quality images of soft tissues. Our study introduced a preoperative planning method using 3D AI-generated lumbar models with 2 key benefits: Enhanced visualization of 3D structures through automated segmentation of preoperative MR images and cost-effectiveness, requiring only C-arm fluoroscopy and our planning plugin, without needing additional machines.

3D models greatly benefit preoperative planning for TP by improving anatomical visualization, which is crucial for precise needle placement in spinal interventions in order to prevent complications and ensure safety. 2D radiography may fail to reveal an obstruction from the L5 transverse process and a hypertrophic L5/S1 facet joint, complicating trajectory planning at the L5/S1 level because of bony obstacles such as the iliac crest and facet joint (14,23). Consequently, many preoperative planning tools based on 3D models have been developed and used in lumbar puncture to assist surgeons in determining the best needle path for each patient (24–27).

Preoperative planning tools make puncture and cannula placement easy and reliable. They can significantly reduce the time required to establish channels for surgery and fluoroscopy in percutaneous endoscopic lumbar discectomy (25). However, the 3D models in previous preoperative planning tools were mostly created manually from CT images. This has 2 significant limitations: it may impede the advancement of preoperative planning for TP, and manual

segmentation of lumbar structures to create 3D models is labor intensive and time consuming, limiting the use of preoperative planning tools. Moreover, lumbar nerve roots are difficult to segment on CT images because of poor soft tissue image quality. To address these limitations, we combined our previously developed automated MR image segmentation for 3D lumbar models (15) with a new planning plugin to enhance the accuracy and efficiency of the TP process.

In our phantom study, the preoperative planning method based on 3D AI-generated lumbar models for TP resulted in significantly shorter puncture times and fewer errors than the conventional fluoroscopy method. Our preoperative planning method for TP resulted in a mean puncture time of 7.29 (SD, 0.95) minutes, longer than the mean 2.97 (SD, 0.56) minutes reported in a study using volume navigation with the fusion of real-time ultrasound and CT images (20). The difference in the guiding methods likely accounted for the time discrepancy. In addition to Liu, et al's (20) method, the timing of image registration should be taken into consideration (the mean time for image registration was 19.13 [SD, 4.94] minutes. Notably, the mean puncture error of our method (3.33 [SD, 0.73 mm]) is approximately the same as that found in the volume navigation study (20). Due to a foramen height of about 21 mm, the puncture error in our preoperative planning method for TP was less than 5 mm, which is acceptable (20,28).

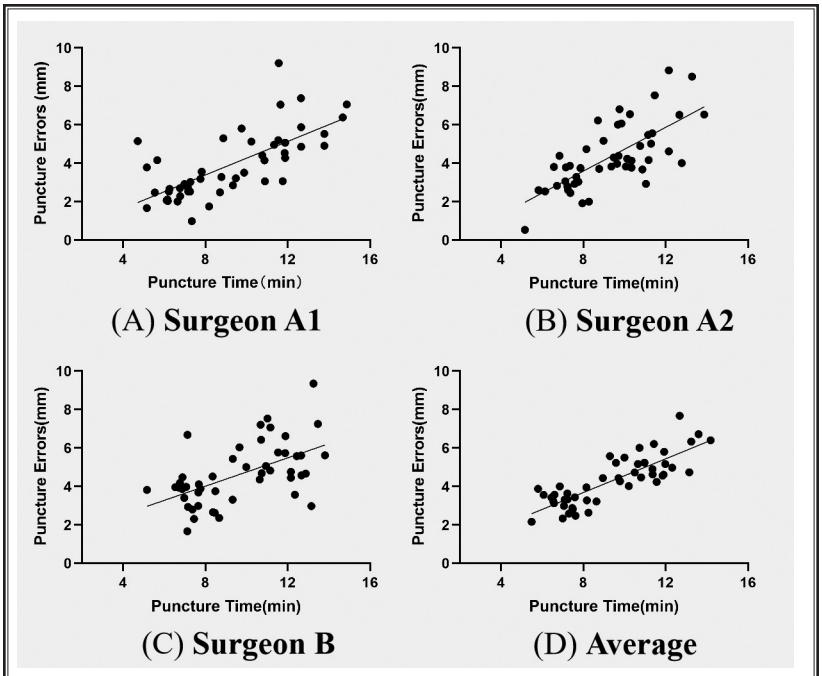

Fig. 4. *Correlation analysis of puncture errors and puncture time. A: correlation analysis of puncture errors and puncture time for surgeon A1; B: correlation analysis of puncture errors and puncture time for surgeon A2; C: correlation analysis of puncture errors and puncture time for surgeon B; D: correlation analysis of average puncture errors and average puncture time.*

Limitations

Our phantom study has some limitations. First, our results are based upon a small number of models, which should be verified using a larger number of models in future studies. The study was also conducted on a phantom, which differs in softness from human tissue. This implies that altering the direction of the needle under the skin would not be the same. Accordingly, additional clinical trials are required to validate our preoperative planning methods.

Table 5. *Test-retest reliability and interobserver reliability of puncture time and puncture error for the 2 methods.*

Accuracy and efficiency	CF (n = 24)	PP (n = 24)	*P* Value
Puncture time (min)			
Surgeon A1	11.60 ± 1.63	6.75 ± 1.10	*P*<0.001
Surgeon A2	11.05 ± 1.24	7.58 ± 1.12	*P*<0.001
Surgeon B	11.79 ± 1.13	7.54 ± 0.95	*P*<0.001
Average	11.48 ± 1.27	7.29 ± 0.95	*P*<0.001
Puncture error (mm)			
Surgeon A1	5.00 ± 1.63	2.81 ± 1.02	*P*<0.001
Surgeon A2	5.14 ± 1.57	3.53 ± 1.46	*P*<0.001
Surgeon B	5.62 ± 1.41	3.64 ± 1.06	*P*<0.001
Average	5.25 ± 0.92	3.33 ± 0.73	*P*<0.001

Unless otherwise stated, data are means (SDs). n = transforaminal puncture trials, CF = the conventional fluoroscopy method, PP = the preoperative planning method. A P value < 0.05 was considered indicative of statistical significance.

Conclusion

The preoperative planning method for TP performed using a phantom is more accurate and efficient

than the conventional fluoroscopic method. Although the present study lacks validation with clinical samples, we demonstrated the potential of planning a suitable pathway for spinal intervention, such as transforaminal epidural steroid injections.

Contribution Statement

Planning: Zhihai Su; Chengjie Huang and Zhifei Cui

Conduct: Zhihai Su; Yunfei Wang; Wencong Zhang; Lei Zhao and Shumao Pang

Reporting: Zhihai Su; Chengjie Huang; Naiwen Zhang and Libin Liang and Hai Lu

Conception and design: Zhihai Su; Chengjie Huang; Zhifei Cui;Zhen Yuan; Qianjin Feng; Xiang Liu; Tao Chen and Hai Lu

Data acquisition: Wencong Zhang; Lei Zhao; Shumao Pang and Zhifei Cui

Data analysis: Naiwen Zhang; Libin Liang; Xiang Liu and Tao Chen

Availability of Data and Materials

The datasets generated and analyzed during the current study are not publicly available, but may be available from one of the corresponding authors upon reasonable request.

Ethics Approval and Consent to Participate

Medical ethics committee approval was obtained for this study (Ethics Number: 2020 K05-1). Due to the secondary data analysis from patients' magnetic resonance images, additional informed consent was not required.

References

1. Stout A, Omar IM, Benzon HT. Preferred insertion site for transforaminal epidural steroid injections: Safe Triangle or Kambin's Triangle? *Anesth Analg* 2023; 137:1135-1138.
2. Doshi TL, Engle AM, Przybysz AJ, Nelson AM. Pro-con debate: Superior versus inferior triangle needle placement in transforaminal epidural injections. *Anesth Analg* 2023; 137:1139-1146.
3. Michalik AJ, Patel RK. Evaluation of transforaminal epidural steroid injections for discogenic axial lumbosacral back pain utilizing PROMIS as an outcome measure. *Spine J* 2021; 21:202-211.
4. Fanous AA, Tumialán LM, Wang MY. Kambin's Triangle: Definition and new classification schema. *J Neurosurg Spine* 2020; 32:390-398.
5. Su Z, Wang M, Zhao Q, et al. Clinical anatomy and possible clinical significance of the intervertebral vein in the lumbar intervertebral foramina. *Pain Physician* 2019; 22:E225-E232.
6. Lee K, Lee KM, Park MS, Lee B, Kwon DG, Chung CY. Measurements of surgeons' exposure to ionizing radiation dose during intraoperative use of C-arm fluoroscopy. *Spine (Phila Pa 1976)* 2012; 37:1240-1244.
7. Oliveira CB, Maher CG, Ferreira ML, et al. Epidural corticosteroid injections for lumbosacral radicular pain. *Cochrane Database Syst Rev* 2020; 4:CD013577.
8. Patel PD, Canseco JA, Houlihan N, Gabay A, Grasso G, Vaccaro AR. Overview of minimally invasive spine surgery. *World Neurosurg* 2020; 142:43-56.
9. Nagamatsu M, Maste P, Tanaka M, et al. Usefulness of 3D CT/MRI fusion imaging for the evaluation of lumbar disc herniation and Kambin's Triangle. *Diagnostics (Basel)* 2022; 12:956.
10. Beach IR, D'Agostino EN, Thakrar R, et al. Learning by drawing and modeling: Teaching modalities for spinal anatomy in medical students. *Anat Sci Educ* 2023; 16:1041-1045.
11. Jecklin S, Shen Y, Gout A, et al. Domain adaptation strategies for 3D reconstruction of the lumbar spine using real fluoroscopy data. *Med Image Anal* 2024; 98:103322.
12. Liu Z, Su Z, Wang M, et al. Computerized characterization of spinal structures on MRI and clinical significance of 3D reconstruction of lumbosacral intervertebral foramen. *Pain Physician* 2022; 25:E27-E35.
13. Chen Z, Guo L, Zhang R, Fang Z, He X, Wang J. BX2S-Net: Learning to reconstruct 3D spinal structures from bi-planar X-ray images. *Comput Biol Med* 2023; 154:106615.
14. Huang X, Zhu B, Liu X. Quantitative 3D trajectory measurement for percutaneous endoscopic lumbar discectomy. *Pain Physician* 2018; 21:E355-E365.
15. Su Z, Liu Z, Wang M, et al. Three-dimensional reconstruction of Kambin's Triangle based on automated magnetic resonance image segmentation. *J Orthop Res* 2022; 40:2914-2923.
16. Fan G, Liu H, Wang D, et al. Deep learning-based lumbosacral reconstruction for difficulty prediction of percutaneous endoscopic transforaminal discectomy at L5/S1 level: A retrospective cohort study. *Int J Surg* 2020; 82:162-169.
17. Zhu Z, Liu E, Su Z, et al. Three-dimensional lumbosacral reconstruction by an artificial intelligence-based automated MR image segmentation for selecting the approach of percutaneous endoscopic lumbar discectomy. *Pain Physician* 2024; 27:E245-E254.
18. Fan G, Gu X, Liu Y, et al. Lower learning difficulty and fluoroscopy reduction of transforaminal percutaneous endoscopic lumbar discectomy with an accurate preoperative location method. *Pain Physician* 2016; 19:E1123-E1134.
19. Wei S, Tao W, Zhu H, Li Y. Three-dimensional intraoperative imaging with O-arm to establish a working trajectory in percutaneous endoscopic lumbar discectomy. *Wideochir Inne Tech Maloinwazyjne* 2016; 10:555-560.
20. Liu Y-B, Wang Y, Chen Z-Q, et al. Volume navigation with fusion of real-time ultrasound and CT images to

guide posterolateral transforaminal puncture in percutaneous endoscopic lumbar discectomy. *Pain Physician* 2018; 21:E265-278.

21. Depriester C, Setbon S, Larde A, Malaquin E, Vanden Abeele B, Bocquet J. CT-guided transforaminal cervical and lumbar epidural injections. *Diagn Interv Imaging* 2012; 93:704-710.
22. Li G, Patel NA, Hagemeister J, et al. Body-mounted robotic assistant for MRI-guided low back pain injection. *Int J Comput Assist Radiol Surg* 2020; 15:321-331.
23. Jiang Y, Wang R, Chen C. Preoperative simulation of the trajectory for L5/S1 percutaneous endoscopic transforaminal discectomy: A novel approach for decision-making. *World Neurosurg* 2021; 145:77-82.
24. Chen X, Cheng J, Gu X, Sun Y, Politis C. Development of preoperative planning software for transforaminal endoscopic surgery and the guidance for clinical applications. *Int J Comput Assist Radiol Surg* 2015; 11:613-620.
25. Hu Z, Li X, Cui J, et al. Significance of preoperative planning software for puncture and channel establishment in percutaneous endoscopic lumbar DISCECTOMY: A study of 40 cases. *Int J Surg* 2017; 41:97-103.
26. Shi C, Sun B, Tang G, et al. Clinical and radiological outcomes of endoscopic foraminoplasty and decompression assisted with preoperative planning software for lumbar foraminal stenosis. *Int J Comput Assist Radiol Surg* 2021; 16:1829-1839.
27. Peng W, Li L, Liang L, et al. A convenient and stable vertebrae instance segmentation method for transforaminal endoscopic surgery planning. *Int J Comput Assist Radiol Surg* 2021; 16:1263-1276.
28. Cinotti G, De Santis P, Nofroni I, Postacchini F. Stenosis of lumbar intervertebral foramen: Anatomic study on predisposing factors. *Spine (Phila Pa 1976)* 2002; 27:223-229.